Ionization of coherent excitons by strong terahertz fields

B. Ewers, N. S. Köster, R. Woscholski, M. Koch, and S. Chatterjee
Faculty of Physics and Materials Sciences Center, Philipps-Universität Marburg, Renthof 5, D-35032 Marburg, Germany

G. Khitrova and H. M. Gibbs
College of Optical Sciences, The University of Arizona, 1630 E. University Boulevard, Tucson, Arizona 85719-0094, USA

A. C. Klettke, M. Kira, and S. W. Koch
Faculty of Physics and Materials Sciences Center, Philipps-Universität Marburg, Mainzer Gasse 33, D-35032 Marburg, Germany
(Received 7 December 2011; revised manuscript received 16 January 2012; published 6 February 2012)

The interaction of coherent excitons with intense, single-cycle terahertz (THz) pulses is investigated. A significant bleaching of the 1*s*-exciton resonance develops into a splitting of the absorption peak and the emergence of pronounced wings with increasing THz field strength. A quantum-mechanical many-body analysis attributes the experimental observations to a transition from excitonic Rabi flopping to multi-THz-photon ionization and the population of optically dark exciton states with high quantum numbers.

DOI: 10.1103/PhysRevB.85.075307 PACS number(s): 78.67.De, 42.65.Re, 78.47.D−

I. INTRODUCTION

The observation and analysis of sophisticated coherent effects in atoms[1,2] has often stimulated the search for similar features in solid-state systems. Direct-gap semiconductors exhibit analogous atomic features through the hydrogenlike series of optically induced exciton resonances. These "coherent excitons," also known as the "coherent excitonic polarization," represent a superposition state of electrons in the conduction band and holes in the valence band with the driving light field.[3] Through the many-body interactions in the system, the coherent excitons can be converted into a quasiparticlelike, incoherent exciton population.[4–6]

With the help of additional fields in the range of the terahertz (THz) part of the electromagnetic spectrum, transitions between different excitonic states can be induced and the nature of the many-body configuration can be identified.[7] Experimental studies of optical-pump and THz-probe experiments have been reported and exciton populations, electron-hole plasma signatures, plasmonic features, as well as nonperturbative exciton bleaching and high-harmonic generation have been identified.[8–10] Using the strong THz fields of a free-electron laser, effects such as photoluminescence quenching of magnetoexcitons[11] or the coupling of states in quantum wells[12] have been studied and recently, excitonic Rabi splitting has been demonstrated.[13]

In this paper, we investigate the interaction of coherent excitons with strong single-cycle THz pulses with the goal to identify exciton ionization features: by systematically controlling the THz photon fluency, we monitor the system response all the way from the weakly coupled perturbative regime into the realm of extreme nonlinear THz optics. Our studies can be viewed as the quasiparticle analogy to the above-threshold ionization scenario in atomic systems,[14] thus, significantly expanding on earlier THz experiments in semiconductor systems.[10,13,15]

II. EXPERIMENTAL SETUP

A regenerative Ti:sapphire amplifier system emitting 800-nm, 120-fs pulses at a 1-kHz repetition rate is used as a light source to excite a commercially available GaAs-based large-area THz emitter. It generates the strong, approximately 1-ps-long single-cycle THz pulses covering nearly three octaves of bandwidth (Fig. 1). Using two off-axis parabolic mirrors, the THz field is imaged onto a semiconductor quantum-well (QW) structure containing 30 $Ga_{0.97}In_{0.03}As$ QWs separated by GaAs barriers (DBR13) which is mounted inside a He-flow microscopy cryostat equipped with polymethylpentene (TPX) windows. The THz field coherently manipulates the 1*s* polarization in the sample and another pair of off-axis parabolic mirrors is used to relay the transmitted THz field onto a 0.8-mm-thick ⟨110⟩-cut ZnTe crystal used for standard electro-optical sampling.[16,17] The THz beam path is kept in an encapsulated environment with a constant-flow nitrogen purge eliminating most water vapor. The peak electric field is set by varying the voltage biasing the THz emitter while keeping the spatial, spectral, and temporal field distribution constant. A THz field strength of up to 15 kV/cm in free space is measured by using a calibrated Golay cell and a knife-edge test at the position of the sample without the cryostat window.

A white-light supercontinuum pulse generated in a ⟨0001⟩-cut sapphire crystal is used as a probe. Its light is transmitted through the sample coaxially to the THz pulse by propagating through 2-mm holes drilled through the 2″-diameter off-axis parabolas. The spectrum of the transmitted optical pulse is dispersed using a grating spectrometer with a resolution of 0.014 nm and detected by a liquid-nitrogen-cooled charge-coupled device camera. This configuration is also used to determine the linear absorption of the sample in transmission geometry as the multiple QW stack is antireflection coated for the 1*s*-exciton energy at cryogenic temperatures. The thickness of approximately 100 nm of the coating is significantly smaller than the THz wavelength used in this experiment and is, therefore, transparent for the THz regime.

III. EXPERIMENTAL RESULTS

The central experimental observations are summarized in Figs. 2 and 3. Figure 2(a) displays the absorption spectra αL with (dark red) and without (light gray) the presence of the

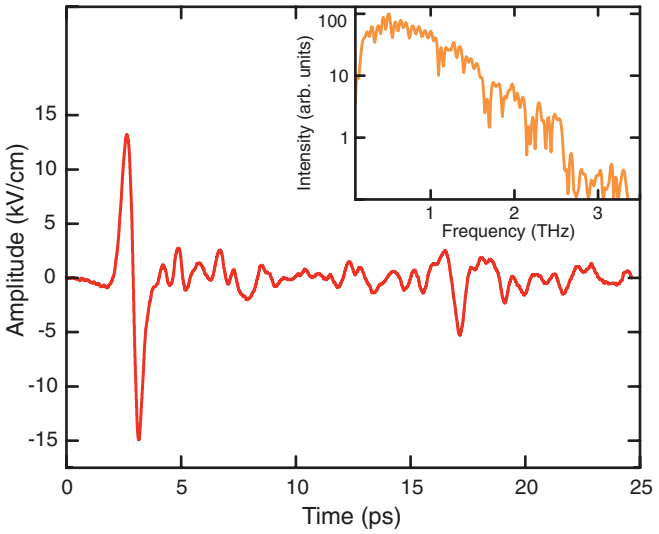

FIG. 1. (Color online) Temporal distribution of the used THz pulses and the corresponding spectrum (inset). The time trace is measured with a standard electro-optical sampling setup based on a 0.8 mm ⟨110⟩-cut ZnTe crystal. The THz field strength of up to 15 kV/cm in free space is measured by using a calibrated Golay cell and a knife-edge test without the cryostat windows.

THz pulse for zero time delay, resulting in the maximum THz-induced changes. We find a pronounced bleaching and splitting of the 1*s*-exciton resonance as well as the development of wings at energies above and below the two central peaks. The strong modulations of about 10–15 meV above the 1*s*-exciton resonance are signatures of high-harmonic generation during Rabi flopping of the 1*s*-2*p* transition.[10,18]

The time evolution of the measured absorption spectrum αL is given in Fig. 2(b) as the contour plot. Note that the sample is transparent to the THz field when no optical polarization is injected. The THz-induced splitting is observed for times in the range of several hundreds of femtoseconds around time zero indicated by the black horizontal line; the position of the main peak(s) is (are) indicated by the dashed white line(s). The alternating structure around 1.5 eV again results from higher THz harmonics.

Figure 2(c) shows the changes of the absorption $\Delta\alpha L_{\text{peak}}$ as a function of time delay at the peak energy of the 1*s*-exciton resonance (1.4919 eV) (solid line). The field amplitude of the single-cycle THz pulse is given as a reference (dashed line). We see that the presence of the THz pulse changes $\Delta\alpha L$ by -3 and change occurs only as long as the THz pulse is present.

The measured intensity dependence of the THz-induced spectral changes at zero time delay for a series of THz field strengths is shown in the left-hand side of Fig. 3(a). We clearly see the gradual transition from weak bleaching of the 1*s*-exciton resonance to a double-peaked spectrum as the THz field strength is increased. For even higher THz intensities, a highly asymmetric spectrum develops featuring pronounced wings on both the low- and high-energy sides of the main peaks.

In Fig. 3(b), the energies of the Rabi-peak resonances are plotted as a function of the THz field strength. We observe the transition from THz-induced exciton bleaching to a pronounced peak splitting which is accompanied by a

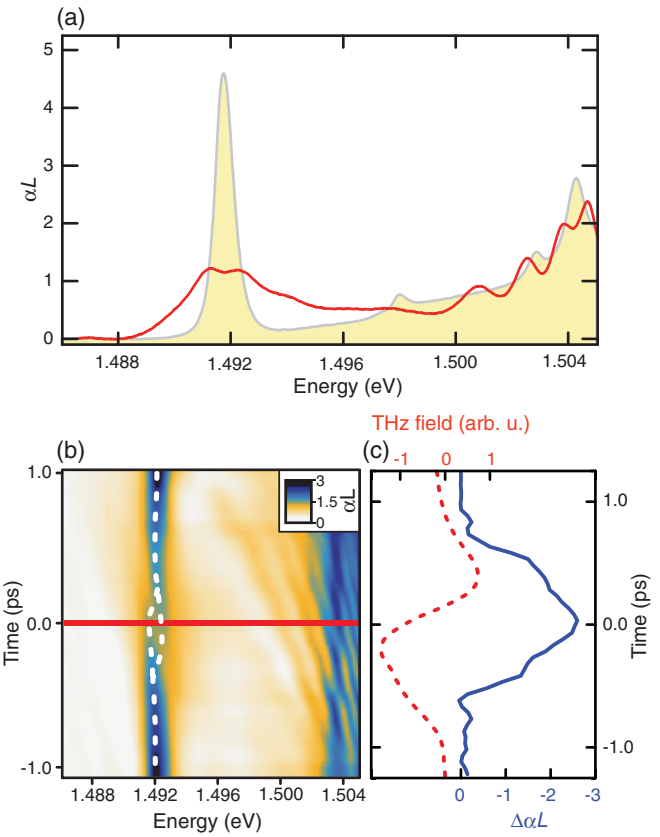

FIG. 2. (Color online) (a) Linear absorption spectrum (red) and absorption under THz radiation at time zero (shaded area). (b) Contour plot of the measured absorption spectrum αL as a function of energy and time delay on a gray scale. The position of the main peak(s) is (are) indicated by the vertical dashed white line(s) acting as a guide(s) to the eye; the red solid line indicates time zero. (c) Peak absorption change $\Delta\alpha L_{\text{peak}}$ at the energy of the 1*s*-exciton resonance in the linear spectrum (solid line); the THz pulse is given as a reference (dashed line).

slight redshift of the spectrum. The energy separation between the split peaks increases linearly with the THz-field amplitude E_{THz} from ∼2.5 to ∼6.0 kV/cm. For high THz amplitudes, the spectrum becomes very broad and the remaining spectra are blueshifted as the THz field is increased. The same features are identified when considering the peak heights in Fig. 3(c). For weak intensities, the absorption peak changes only moderately. After the split peaks emerge at intermediate intensities, the absorption peak starts to decrease rapidly as excitation is increased. For high excitations, both the absorption peak and the splitting saturate, whereas the spectrum develops extended wings.

IV. THEORY

A detailed understanding of the underlying mechanism is achieved by applying a systematic analysis using a microscopic many-body theory. The approach self-consistently includes the optical and the THz fields as well as the microscopic quasiparticle interactions for the analysis of these effects.[10,18–20] Starting from the standard many-body

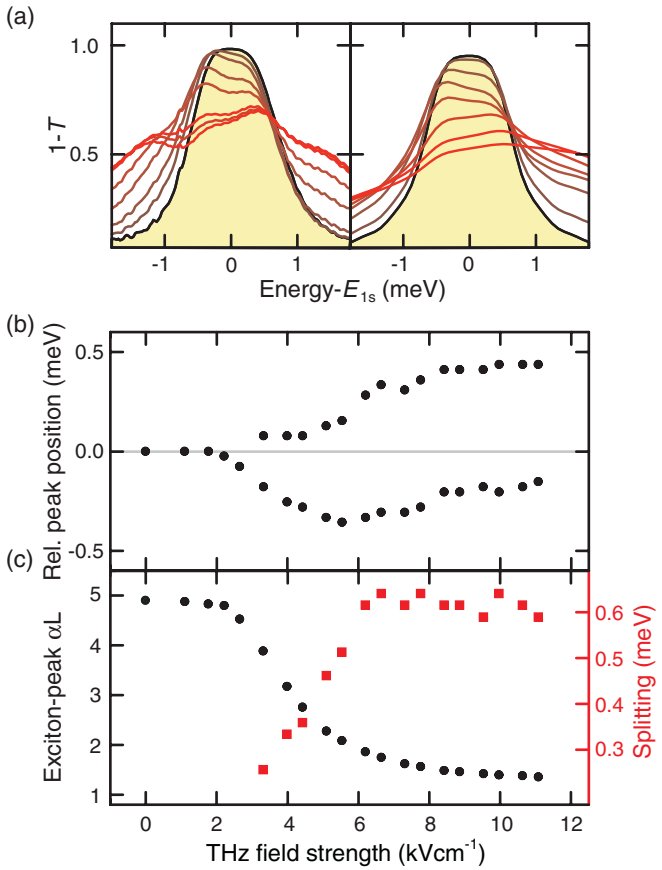

FIG. 3. (Color online) (a) Measured (left) and calculated (right) transmission data $(1-T)$ for various applied THz field strength at time zero: 0, 1.6, 3.2, 4.8, 6.4, 8.0, 9.6, 11.2, and 12.8 kV/cm (from top, gray, to bottom, red). (b) Peak energies relative to the $1s$-exciton resonance in the unperturbed system. (c) Peak absorption (black dots) and splitting of the $1s$-exciton resonance (squares).

Hamiltonian for Coulomb-interacting carriers which couple to light via the minimal substitution Hamiltonian, the dynamic equation for the polarization dynamics is derived using the systematic cluster-expansion approach:[3]

$$i\hbar\frac{\partial}{\partial t}P_{\mathbf{k}} = \left(\epsilon_{\mathbf{k}} - j_{\mathbf{k}}A_{\mathrm{THz}} + \frac{|e|^2}{2\mu}A_{\mathrm{THz}}^2\right)P_{\mathbf{k}} + \sum_{\mathbf{k}'}\Gamma_{\mathbf{k},\mathbf{k}'}P_{\mathbf{k}'} - \left(1-f_{\mathbf{k}}^e-f_{\mathbf{k}}^h\right)\left(d_{cv}E_{\mathrm{opt}} + \sum_{\mathbf{k}'}V_{\mathbf{k}-\mathbf{k}'}P_{\mathbf{k}'}\right). \quad (1)$$

Here, the first set of parentheses contains the sum of the kinetic carrier energies $\epsilon_{\mathbf{k}}$, the THz current $j_{\mathbf{k}}A_{\mathrm{THz}}$, where A_{THz} is the vector potential of the THz field and $j_{\mathbf{k}}$ is the current-matrix element, as well as the so-called ponderomotive current $\frac{|e|^2}{2\mu}A_{\mathrm{THz}}^2$. The second term, $\sum_{\mathbf{k}'}\Gamma_{\mathbf{k},\mathbf{k}'}P_{\mathbf{k}'}$, describes excitation-induced dephasing due to Coulomb and phonon scattering. The last term is the usual product of the phase-space filling factor $1-f_{\mathbf{k}}^e-f_{\mathbf{k}}^h$ times the generalized optical Rabi frequency $d_{cv}E_{\mathrm{opt}}+\sum_{\mathbf{k}'}V_{\mathbf{k}-\mathbf{k}'}P_{\mathbf{k}'}$ (Ref. 21) containing the optical field E_{opt} and the dipole-matrix element d_{cv}.

The total electromagnetic field $E(z,t) = E_{\mathrm{opt}}(z,t) + E_{\mathrm{THz}}(z,t)$ for light propagating perpendicular to the QWs and polarized linearly in the x direction is determined from the wave equation

$$\left[\frac{\partial^2}{\partial z^2} - \frac{n^2(z)}{c_0^2}\frac{\partial^2}{\partial t^2}\right]E(z,t) = \mu_0\left(\frac{\partial^2 P_{\mathrm{opt}}(z)}{\partial t^2} + \frac{\partial J(z)}{\partial t}\right), \quad (2)$$

where $P_{\mathrm{opt}} \sim \sum_{\mathbf{k}} P_{\mathbf{k}}$ and J is the sum of THz and ponderomotive currents. The refractive index profile of the system is determined by $n(z)$. The THz contribution satisfies $E_{\mathrm{THz}} = -\frac{\partial}{\partial t}A_{\mathrm{THz}}$.

To monitor the THz-induced transitions between excitonic states, we apply the projection

$$p_\lambda = \sum_{\mathbf{k}}\phi_\lambda^\star(\mathbf{k})\,P_{\mathbf{k}}, \quad (3)$$

where $\phi_\lambda^\star(\mathbf{k})$ is the wave function of the Wannier exciton.[21] The probability to detect the exciton component λ is then defined by $n_\lambda = |p_\lambda|^2$. For QW systems, $\lambda = (n,m)$ is uniquely defined by the principal quantum number n and the orbital quantum number m. The combination $\lambda = (1,0)$ defines the $1s$ state and $\lambda = (2,\pm1)$ identifies the $2p$ state, respectively.

V. ANALYSIS

Results from the full calculation are shown on the right-hand side of Fig. 3(a) for a sequence of THz field strengths. Very good agreement with the experimental data is observed. All the relevant features, such as the increasing bleaching and the growing splitting of the $1s$-exciton resonance with increasing field strength, are clearly observable both in the calculated and the measured data. Furthermore, a slight redshift is obtained for weak THz field strength, which changes into a clear blueshift for stronger fields.

For a more detailed analysis, we present the computed results for the field strengths of 4.8 (left) and 9.6 kV/cm (right) in Fig. 4. These are representative for the medium and high-field excitation situations of the data summarized in Fig. 3. The black solid line indicates the results of the full microscopic calculation and the orange solid line is obtained for a two-level calculation, where only the excitonic $1s$ and $2p$ states are included. As a reference, the shaded area shows the absorption without the THz pump. For the lower THz field strength of 4.8 kV/cm, the two-level calculation [solid orange line in the left panel of Fig. 4(a)] seems to capture the main aspects of the Rabi splitting. However, the relatively good agreement with the full calculation is somewhat incidental as evidenced by the reference calculation for a slightly increased THz field of 5.1 kV/cm. Whereas the full calculation (not shown) is virtually indistinguishable from the 4.8 kV/cm result, the two-level result produces a dramatic change due to its phase sensitivity [cf. Fig. 4(a), as outlined below].

Whereas the failure of the two-level approximation for strong THz fields is not really surprising,[13] its comparison with the full calculation allows us to identify the characteristic high-field signatures. For this purpose, we show in Fig. 4(b) the temporal development of the excitonic occupations n_λ in the different states, using the full model (top frames) and the two-level approximation (bottom frames). Without the THz field (shaded area), the optically induced n_{1s} decays single

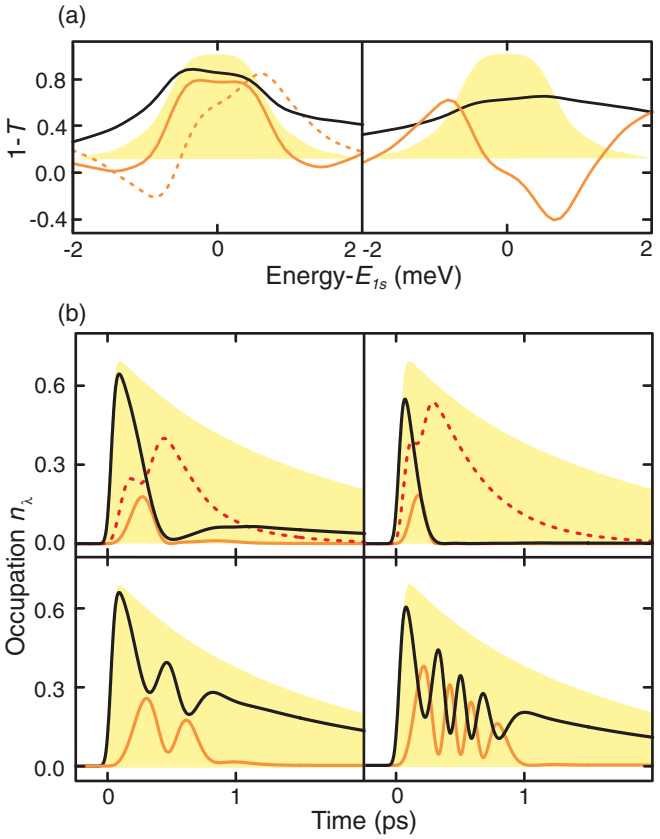

FIG. 4. (Color online) Computed THz-induced effects for 4.8 (left) and 9.6 kV/cm (right) fields. (a) The microscopically computed transmission, plotted as $1 - T$, is shown as a solid black line, and the corresponding result of a two-level analysis is shown as an orange line. The dashed line in the top left panel corresponds to a two-level calculation for a slightly larger THz field of 5.1 kV/cm. The spectra without THz are shown as shaded areas. (b) Time evolution of the $1s$ state (black line), the $2p$ state (orange line), and all other dark states (dashed line) of the polarization are shown as obtained from the full computation (top frames) and the two-level calculation (bottom frames). The shaded area indicates the decaying $1s$ polarization without the THz perturbation.

exponentially. Including the THz field, the $1s$ occupation shows signs of Rabi flopping. For relatively low THz intensities (left), most of the $1s$ excitation is transferred to the $2p$ (orange line) and higher states (dashed line) before some part of it returns back to the $1s$ state (solid line), indicating reversible population transfer. Such a revival of the $1s$ polarization does not occur for strong THz fields (right), because the $1s$ polarization is completely converted into higher states after about 400 fs such that the $1s$ component does not recover. In contrast, the two-level results in the bottom frames of Fig. 4(b) always show pronounced Rabi flopping and reversible population transfer. The rapid oscillations indicate the strong phase sensitivity between the THz-induced $1s$ and $2p$ polarization components which are responsible for the dramatically different results for slightly different THz-field strengths [left frame in Fig. 4(a)].

In order to analyze the results of the strong THz excitation and to identify the roles of the individual exciton states, we investigate the relative occupation probabilities n_λ of the

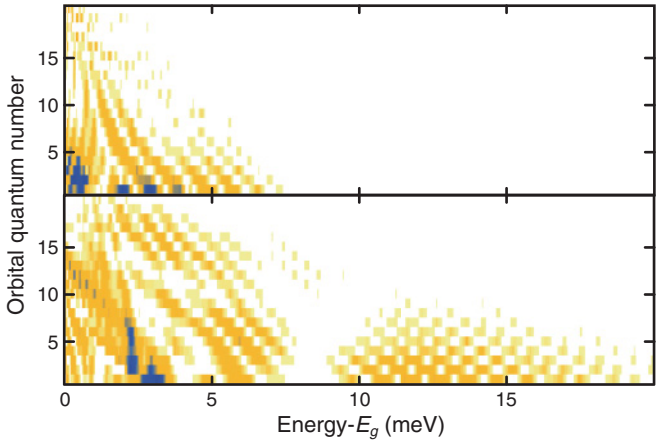

FIG. 5. (Color online) Relative occupation probabilities of the ionized excitonic states as function of energy and orbital quantum number. The computed n_λ are defined as 1.5 ps after 4.8- (top) and 9.6-kV/cm (bottom) excitations analyzed in Fig. 4.

ionized exciton states as a function of the energy and orbital quantum number at the time of 1.5 ps after the THz excitation shown in Fig. 5.

We see that the THz pulse transfers the optically induced $1s$ occupation into states with energies corresponding to more than 4 THz photons and high orbital quantum numbers. This effect can be considered as the THz analogy to the above-threshold ionization of atomic systems[14] mentioned above. The excitation transfer into ionized excitonic states eliminates the phase sensitivity responsible for the failure of the two-level calculations shown in Fig. 4. In the spectrum shown in Fig. 3(a), the ionization effects lead to the appearance of pronounced wings. While significant exciton-ionization effects are observed for both exemplary THz excitations considered here, these become extremely dominant for the strong THz fields shown in the bottom panel.

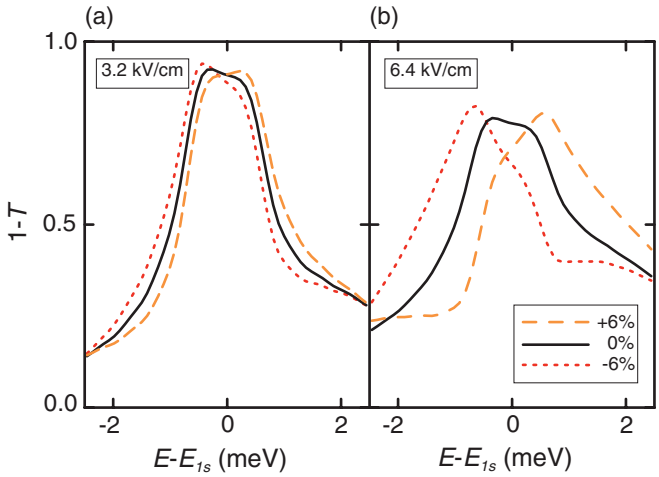

FIG. 6. (Color online) Effect of the THz-induced ponderomotive contribution on the optical transmission. The THz field has the strength of (a) 3.2 and (b) 6.4 kV/cm and the ponderomotive contribution is changed by −6% (dotted line), 0% (solid line), and 6% (dashed line) with respect to the actual value.

To investigate the influence of the ponderomotive current on the peak positions, we systematically vary the original ponderomotive current in Eq. (1) by a factor s. This allows us to either enhance ($s > 1$) or suppress ($s < 1$) the ponderomotive effects in the computations. Figure 6 compares the original ($s = 1$, solid line) transmission spectrum with enhanced ($s = 1.06$, dashed line) and suppressed ($s = 0.94$, dotted line) ponderomotive effects. The left column is computed with a THz field of 3.2 kV/cm that corresponds to the onset of Rabi splitting in Fig. 3. The right column is calculated with 6.4 kV/cm corresponding to the saturation regime, according to Fig. 3.

In both cases, increasing ponderomotive contributions produces a blueshift of the resonances. Whereas this shift is relatively small for THz fields close to the Rabi-splitting threshold, it becomes considerably larger for elevated E_{THz}. This behavior follows from the quadratic A_{THz} dependency of J_{pond}. Due to this blueshift, the ponderomotive contributions produce the asymmetric shift of the low- and high-energy branch of the Rabi peak, observed in Fig. 3(b).

VI. CONCLUSIONS

In summary, we investigated the interaction of strong single-cycle, broadband THz pulses with optically generated coherent excitons in $Ga_{0.97}In_{0.03}As/GaAs$ QWs. By monitoring the optical response for increasing THz-field strengths, we see the gradual transition from bleaching of the 1s-exciton resonance into Rabi splitting and the development of pronounced wings. The slight absorption redshift for weak THz field strengths turns into a blueshift when stronger fields are applied. Our quantum-mechanical many-body analysis attributes the experimental observations to excitonic Rabi flopping supplemented by multi-THz-photon ionization and the population of optically dark exciton states with high quantum numbers.

ACKNOWLEDGMENTS

S.C. and N.K. acknowledge stimulating discussions with W. W. Rühle.

[1] I. I. Rabi, Phys. Rev. **51**, 652 (1937).
[2] B. R. Mollow, Phys. Rev. **188**, 1969 (1969).
[3] M. Kira and S. Koch, Prog. Quantum Electron. **30**, 155 (2006).
[4] S. Chatterjee, C. Ell, S. Mosor, G. Khitrova, H. M. Gibbs, W. Hoyer, M. Kira, S. W. Koch, J. P. Prineas, and H. Stolz, Phys. Rev. Lett. **92**, 067402 (2004).
[5] M. Kira and S. W. Koch, Phys. Rev. Lett. **93**, 076402 (2004).
[6] W. Hoyer, C. Ell, M. Kira, S. W. Koch, S. Chatterjee, S. Mosor, G. Khitrova, H. M. Gibbs, and H. Stolz, Phys. Rev. B **72**, 075324 (2005).
[7] S. W. Koch, M. Kira, G. Khitrova, and H. M. Gibbs, Nature Mater. (London) **5**, 523 (2006).
[8] R. Huber, F. Tauser, A. Brodschelm, M. Bichler, G. Abstreiter, and A. Leitenstorfer, Nature (London) **414**, 286 (2001).
[9] R. A. Kaindl, M. A. Carnahan, D. Hägele, R. Lövenich, and D. S. Chemla, Nature (London) **423**, 734 (2003).
[10] J. R. Danielson, Y.-S. Lee, J. P. Prineas, J. T. Steiner, M. Kira, and S. W. Koch, Phys. Rev. Lett. **99**, 237401 (2007).
[11] J. Černe, J. Kono, M. S. Sherwin, M. Sundaram, A. C. Gossard, and G. E. W. Bauer, Phys. Rev. Lett. **77**, 1131 (1996).
[12] S. G. Carter, V. Birkedal, C. S. Wang, L. A. Coldren, A. V. Maslov, D. S. Citrin, and M. S. Sherwin, Science **310**, 651 (2005).
[13] M. Wagner, H. Schneider, D. Stehr, S. Winnerl, A. M. Andrews, S. Schartner, G. Strasser, and M. Helm, Phys. Rev. Lett. **105**, 167401 (2010).
[14] P. B. Corkum, N. H. Burnett, and F. Brunel, Phys. Rev. Lett. **62**, 1259 (1989).
[15] H. Hirori, M. Nagai, and K. Tanaka, Phys. Rev. B **81**, 081305(R) (2010).
[16] Q. Wu and X.-C. Zhang, Appl. Phys. Lett. **67**, 3523 (1995).
[17] P. U. Jepsen, C. Winnewisser, M. Schall, V. Schyja, S. R. Keiding, and H. Helm, Phys. Rev. E **53**, R3052 (1996).
[18] J. T. Steiner, M. Kira, and S. W. Koch, Phys. Rev. B **77**, 165308 (2008).
[19] A. D. Jameson, J. L. Tomaino, Y.-S. Lee, J. P. Prineas, J. T. Steiner, M. Kira, and S. W. Koch, Appl. Phys. Lett. **95**, 201107 (2009).
[20] S. Leinß, T. Kampfrath, K. v. Volkmann, M. Wolf, J. T. Steiner, M. Kira, S. W. Koch, A. Leitenstorfer, and R. Huber, Phys. Rev. Lett. **101**, 246401 (2008).
[21] H. Haug and S. W. Koch, *Quantum Theory of the Optical and Electronic Properties of Semiconductors* (World Scientific, Singapore, 2009).